Andreev bound states at nonmagnetic impurities in superconductor/antiferromagnet heterostructures

G. A. Bobkov,[1] I. V. Bobkova ◉,[1,2] and A. M. Bobkov[1]

[1]*Moscow Institute of Physics and Technology*, Dolgoprudny, 141700 Moscow Region, Russia
[2]*National Research University Higher School of Economics*, 101000 Moscow, Russia

Andreev bound states can occur at single impurities in superconductors if the impurities suppress superconductivity for a given system. In particular, well-known Yu-Shiba-Rusinov states occur at magnetic impurities in conventional *s*-wave superconductors. Here we demonstrate that nonmagnetic impurities in superconductor/antiferromagnet (S/AF) heterostructures with conventional intraband *s*-wave pairing also produce Andreev bound states. Analogously to the Yu-Shiba-Rusinov bound states the bound states in S/AF bilayers are spin split, but the spin of a particular bound state is determined by the sublattice to which the impurity belongs. The standard decay of the bound state local density of states is superimposed by atomic oscillations related to the staggered character of the exchange field in the host material and by another oscillating pattern produced by finite-momentum Néel triplet pairing generated at the impurity.

I. INTRODUCTION

Impurities in superconductors are some of the most important tools for identifying the nature of the pairing state and microscopic properties of superconductors and for realization of topological superconductivity [1–7]. A lot of effort is devoted to investigation of how different types of impurities influence the critical superconducting temperature for different types of superconducting pairing. In conventional *s*-wave superconductors nonmagnetic impurities do not suppress superconductivity according to Anderson's theorem [8]. However, magnetic impurities are pair breaking for conventional *s*-wave superconductors and suppress their critical temperature [1,9]. For unconventional superconductors with anisotropic [1,10] or *s*-wave odd-parity pairing [11–15] even nonmagnetic impurities can be pair breaking.

A related important problem is the study of Andreev bound states, which can occur in the vicinity of single impurities if the impurities suppress superconductivity for a given system. The single-impurity Andreev bound states have attracted much attention over the last several decades [1]. The magnetic impurities break the time-reversal symmetry and for this reason they are pair breaking even for conventional *s*-wave superconductors. Well-known Yu-Shiba-Rusinov states occur at magnetic impurities [16–18]. On chains of magnetic impurities they can form topological bands due to overlapping of bound states at separate impurities [5–7]. For *d*-wave superconductors even nonmagnetic impurities are pair breakers and produce bound states due to the fact that the change of the quasiparticle momentum upon scattering disrupts the phase assignment for particular directions of the momenta in such a pairing state [1,19]. In addition, the nonmagnetic impurities can result in superconductivity suppression and impurity-induced Andreev bound states in multiband superconductors [20–22]. In unconventional superconductors they serve as a test of the pairing symmetry [3,4].

Here we demonstrate that impurity-induced Andreev bound states at *nonmagnetic* impurities can also occur in superconductor/antiferromagnet (S/AF) heterostructures with conventional intraband *s*-wave pairing. The system is sketched in Fig. 1 and represents a thin-film bilayer composed of a superconductor and a two-sublattice antiferromagnet. The general physical argument allowing for the bound state at a nonmagnetic impurity in such a system is the following. The ideal bilayer in the absence of impurities is symmetric under simultaneous action of time reversal and sublattice interchange. The presence of impurity breaks this symmetry. As a result, for conduction electrons the impurity can be viewed as effectively magnetic. Analogously to the Yu-Shiba-Rusinov bound states the bound states in S/AF bilayers are spin split, but the spin of a particular bound state is determined by the sublattice to which the impurity belongs (see Fig. 1 for illustration).

The presence of Andreev bound states at single nonmagnetic impurities in S/AF bilayers is in agreement with the behavior of the superconducting critical temperature of such systems in the presence of random disorder, which has already been studied [23–25]. In Ref. [24] it was shown that nonmagnetic impurities can suppress or *enhance* superconductivity depending on the value of the chemical potential. At $\mu \lesssim T_{c0}$, where T_{c0} is a critical temperature of the superconductor, the nonmagnetic impurities enhance superconductivity of S/AF bilayers. It is connected with the presence of so-called Néel triplet correlations [26], which are destructive to singlet superconductivity in the S layer, but are actually interband correlations and therefore are suppressed by nonmagnetic disorder. In contrast, if $\mu \gg T_{c0}$ the superconductivity is suppressed by nonmagnetic disorder. Here we demonstrate that the same sensitivity to the value of the chemical potential occurs in the problem of a single impurity: the bound states only exist at $\mu \gg T_{c0}$, when the impurities suppress superconductivity.
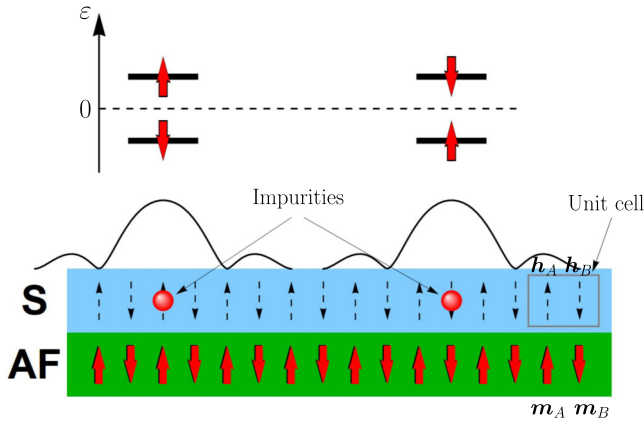
214508-1

FIG. 1. Sketch of the system under consideration. An insulating two-sublattice antiferromagnet (AF) with staggered magnetization $\boldsymbol{m}_A = -\boldsymbol{m}_B$ induces a staggered exchange field $\boldsymbol{h}_A = -\boldsymbol{h}_B$ via the proximity effect in the adjacent thin superconductor (S). The unit cell is shown by a rectangle. An impurity can occupy site A or B in the S layer. Both possible variants are shown by red balls. The LDOS of Andreev bound states localized at the corresponding impurity is shown schematically. The energy spectrum of the bound states with the appropriate spin structure (red arrows) is also shown above the corresponding impurity.

The paper is organized as follows. In Sec. II we describe the considered model and formulate the T-matrix approach generalized for theoretical description of single impurity problems in the two-sublattice formalism. In Sec. III we discuss the dependence of bound state energies on all significant physical parameters and present dependencies of the impurity-induced local density of states (LDOS) on the quasiparticle energy. Section IV is devoted to discussion of the spatial distribution of the LDOS around an impurity. Our conclusions are formulated in Sec. V. The Appendixes provide additional information on the derivation of the two-sublattice T-matrix formalism, phase diagrams of the regions where the bound states exist, and the spin and spatial structure of the impurity-induced LDOS.

II. SYSTEM AND METHOD

In the considered thin-film S/AF bilayer (see Fig. 1) the antiferromagnet is assumed to be an insulator. The magnetism is staggered and the S/AF interface is fully compensated, that is, the interface magnetization has zero average value. The sites in the superconductor are marked by the radius vector $\boldsymbol{r} = (x, y, z)^T$, where x, y, z are integer numbers, and the interface is in the (x, y) plane. The influence of the antiferromagnetic insulator on the thin S layer with thickness smaller than the superconducting coherence length ξ can be described by the Néel-type exchange field $\boldsymbol{h}_{\boldsymbol{r}}^N = (-1)^{x+y+z}\boldsymbol{h}$ [26], which leads to the following effective lattice Hamiltonian of the S layer:

$$\hat{H} = -t \sum_{\langle \boldsymbol{rr'} \rangle, \sigma} \hat{c}_{\boldsymbol{r}\sigma}^\dagger \hat{c}_{\boldsymbol{r'}\sigma} + \sum_{\boldsymbol{r}} (\Delta \hat{c}_{\boldsymbol{r}\uparrow}^\dagger \hat{c}_{\boldsymbol{r}\downarrow}^\dagger + \text{H.c.}) - \mu \sum_{\boldsymbol{r},\sigma} \hat{n}_{\boldsymbol{r}\sigma}$$
$$- \sum_{\boldsymbol{r},\alpha\beta} \hat{c}_{\boldsymbol{r}\alpha}^\dagger (\boldsymbol{h}_{\boldsymbol{r}}^N \boldsymbol{\sigma})_{\alpha\beta} \hat{c}_{\boldsymbol{r}\beta} + \sum_\sigma U_0 c_{\boldsymbol{r}_{\text{imp}},\sigma}^\dagger c_{\boldsymbol{r}_{\text{imp}},\sigma} \quad (1)$$

where $\langle \boldsymbol{rr'} \rangle$ means summation over the nearest neighbors, $\hat{c}_{\boldsymbol{r}\sigma}^\dagger (\hat{c}_{\boldsymbol{r}\sigma})$ is the creation (annihilation) operator for an electron with spin σ at site $\boldsymbol{r}$, t parametrizes the hopping between adjacent sites, and Δ accounts for on-site s-wave pairing. Since the superconducting layer is thin with respect to ξ, Δ and $\boldsymbol{h}$ are assumed to be homogeneous along the z direction. μ is the electron chemical potential, $\hat{n}_{\boldsymbol{r}\sigma} = \hat{c}_{\boldsymbol{r}\sigma}^\dagger \hat{c}_{\boldsymbol{r}\sigma}$ is the particle number operator, $\boldsymbol{\sigma} = (\sigma_x, \sigma_y, \sigma_z)^T$ are Pauli matrices in spin space, the lattice constant is denoted by a, and U_0 is a potential of the single nonmagnetic impurity, which is located at site $\boldsymbol{r}_{\text{imp}}$.

To calculate the bound state energies and LDOS around a single impurity we generalized the T-matrix formalism [1] for taking into account the antiferromagnetic character of the host material. It is done on the basis of the Gor'kov Green's functions in the two-sublattice framework [24,26]. Relegating technical details of the derivations to Appendix A, here we present the resulting equations. In the framework of the two-sublattice formalism we choose the unit cell with two sites belonging to two sublattices A and B, as shown in Fig. 1. The Green's function is a 8×8 matrix in the direct product of spin, particle-hole, and sublattice spaces. Therefore, in addition to the Pauli matrices $\boldsymbol{\sigma} = (\sigma_x, \sigma_y, \sigma_z)^T$ in spin space we define the Pauli matrices $\boldsymbol{\tau} = (\tau_x, \tau_y, \tau_z)^T$ in particle-hole space and $\boldsymbol{\rho} = (\rho_x, \rho_y, \rho_z)^T$ in sublattice space.

In the framework of the T-matrix approach the retarded Green's function takes the form

$$\check{G}_{ii} = \check{G}_{ii}^0 + \check{G}_{ii_{\text{imp}}}^0 \check{T} \check{G}_{i_{\text{imp}}i}^0, \quad (2)$$

where $\boldsymbol{i} \equiv \boldsymbol{r}_A$ is the coordinate of a unit cell coinciding with the radius vector of its A site. $\check{G}_{ij}^0$ is the homogeneous Green's function of the S/AF bilayer in the absence of the impurity and the T matrix takes the form

$$\check{T} = \left(1 - \check{U}_0 \check{G}_{i_{\text{imp}}i_{\text{imp}}}^0\right)^{-1} \check{U}_0 \quad (3)$$

with $\check{U}_0$ being a matrix of impurity potential, which takes the form

$$\check{U}_0 = U_0 \frac{(\rho_x \pm i\rho_y)}{2}. \quad (4)$$

The sign $\pm$ describes the impurity located at a site A (B). For definiteness further we assume that the impurity is located at the A site. The results for impurities located at a site B are obtained by $\boldsymbol{h} \to -\boldsymbol{h}$. Then the bound state energies are determined by the following equation:

$$\det\left(1 - \check{U}_0 \check{G}_{i_{\text{imp}}i_{\text{imp}}}^0\right) = 0, \quad (5)$$

where $\check{G}_{i_{\text{imp}}i_{\text{imp}}}^0$ can be found analytically (see Appendix A), it is diagonal in spin space $\check{G}_{i_{\text{imp}}i_{\text{imp}}}^0 = \check{G}_{i_{\text{imp}}i_{\text{imp}},\uparrow}^0 (1 + \sigma_z)/2 + \check{G}_{i_{\text{imp}}i_{\text{imp}},\downarrow}^0 (1 - \sigma_z)/2$, and its spin-up and spin-down components take the form

$$\check{G}_{i_{\text{imp}}i_{\text{imp}},\sigma}^0 = G_{0x}^\sigma \tau_0 \rho_x + G_{yx}^\sigma \tau_y \rho_x + G_{zx}^\sigma \tau_z \rho_x$$
$$+ G_{0y}^\sigma \tau_0 \rho_y + G_{yy}^\sigma \tau_y \rho_y + G_{zy}^\sigma \tau_z \rho_y, \quad (6)$$

$$G_{0x}^\sigma = \mu[(-h^2 + \Delta^2 - \varepsilon^2 + \mu^2)I_1 - I_2]$$
$$G_{yx}^\sigma = -i\Delta[(-h^2 + \Delta^2 - \varepsilon^2 + \mu^2)I_1 + I_2]$$

$$G_{zx}^{\sigma} = \varepsilon[(-h^2 - \Delta^2 + \varepsilon^2 - \mu^2)I_1 - I_2]$$

$$G_{0y}^{\sigma} = 2ih\sigma\varepsilon\mu I_1$$

$$G_{yy}^{\sigma} = 2h\sigma\Delta\varepsilon I_1$$

$$G_{zy}^{\sigma} = ih\sigma[(h^2 - \Delta^2 - \varepsilon^2 - \mu^2)I_1 + I_2], \quad (7)$$

where ε is a quasiparticle energy, $\sigma = \pm 1$ as a factor in the expression for spin-up (-down) components, $h = |\boldsymbol{h}|$, $I_1 = -\frac{2\sqrt{2}i\pi}{(\alpha_1 + \alpha_2)\alpha_1\alpha_2}$, $I_2 = \frac{\sqrt{2}i\pi}{\alpha_1 + \alpha_2}$, $\alpha_{1,2} = \sqrt{-\beta_1 \mp \sqrt{\beta_1^2 - 4\beta_0}}$, $\beta_0 = h^4 + (\Delta^2 - \varepsilon^2 + \mu^2)^2 - 2h^2(\Delta^2 + \varepsilon^2 + \mu^2)$, and $\beta_1 = 2(\Delta^2 - \varepsilon^2 - \mu^2 + h^2)$.

The superconducting order parameter is taken as $\Delta = 0.1t$ throughout the paper. In principle, it is also disturbed by the pair-breaking impurity and should be calculated self-consistently. But we do not perform the self-consistency procedure, which is a quite standard approximation upon treating single-impurity problems because the suppression of the order parameter is determined by the Fermi wavelength and does not affect the position of the bound state [1].

III. BOUND STATE ENERGIES AND ENERGY-RESOLVED DOS

The LDOS at A and B sublattices can be calculated as

$$N^{A,B}(\varepsilon, \boldsymbol{i}) = -\frac{1}{\pi}\text{Im}\left[\text{Tr}\left[\frac{\check{G}_{ii}(\tau_0 + \tau_z)(\rho_x \pm i\rho_y)}{4}\right]\right]. \quad (8)$$

The LDOS calculated at the impurity site and at the nearest neighbor of the impurity is plotted in Figs. 2(a) and 2(b), respectively. The bound states are represented by the peaks at $\varepsilon = \pm\varepsilon_b$ with asymmetric heights inside the superconducting gap. Higher outer peaks in Fig. 2(b) correspond to the superconducting gap $2E_g^S$. At the impurity site they are fully destroyed by the bound state [see Fig. 2(a)]. The asymmetry of the bound state peaks is connected with the overall particle-hole asymmetry of the LDOS. This asymmetry is clearly seen in the insets, which show the LDOS for a larger energy range. Here we can also see the antiferromagnetic gap $2E_g^{AF}$ at energies $\varepsilon \in [-\mu - h, -\mu + h]$ and an additional peak inside this gap. This peak corresponds to another impurity-induced bound state, which is not related to superconductivity and survives also in the normal state. We do not focus on this nonsuperconducting bound state here.

As it was briefly mentioned in the Introduction, the physical reason for appearance of these bound states is that the impurity in the S/AF host behaves like a magnetic impurity. Below we provide more details about this physical explanation. Energies of the bound states as functions of the impurity strength are plotted in Fig. 3. It is seen that at stronger staggered effective exchange field h the bound state is shifted deeper inside the superconducting gap region. For the chosen set of parameters we cannot consider $h > 0.9\mu = 18\Delta$ because of the overall suppression of superconductivity by the Néel triplet correlations [24]. For comparison the energies of the Yu-Shiba-Rusinov bound states at a magnetic impurity with the same strength in a conventional s-wave superconducting host are plotted by the dashed lines. Unlike the case of magnetic impurity our nonmagnetic impurities in S/AF bilayers are not able to support low- and zero-energy bound
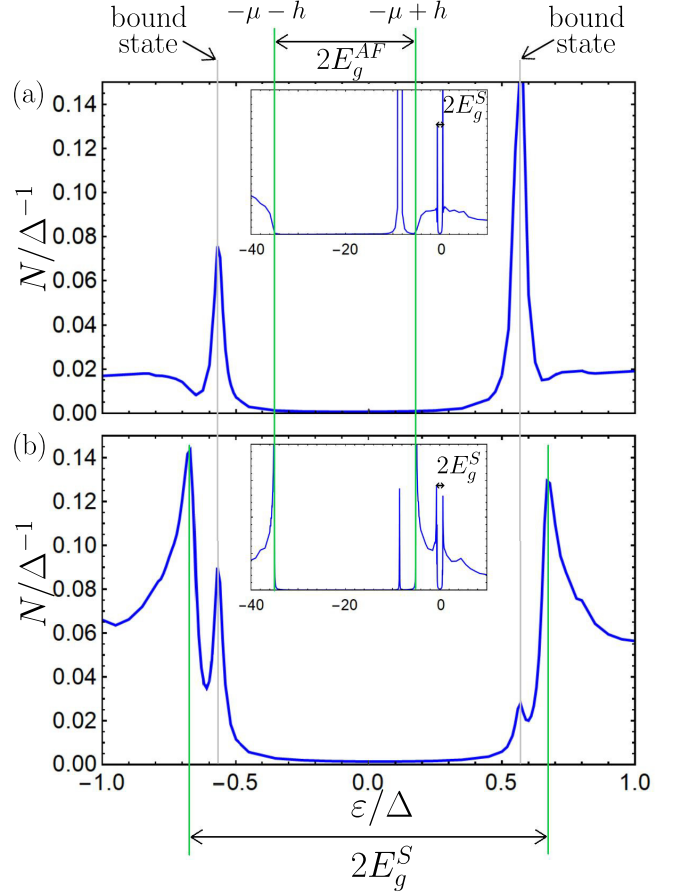

FIG. 2. LDOS as a function of energy. (a) LDOS at the impurity site. (b) LDOS at the nearest neighbor of the impurity. The insets show the same LDOS for larger energy range. $2E_g^S$ is a superconducting gap at the Fermi level. The antiferromagnetic gap $2E_g^{AF}$ at $\varepsilon \in [-\mu - h, -\mu + h]$ and the nonsuperconducting additional bound state inside this gap are also seen. $t = 10\Delta$, $\mu = 20\Delta$, $h = 15\Delta$, $U_0 = 10\Delta$. The Dynes parameter describes the level broadening, $\Gamma = 0.02\Delta$ (see Appendix A for description).

states. In this sense one can say that they are weaker pair breakers as compared to the magnetic impurities.

All the results discussed above are related to the case of strong chemical potential $\mu = 20\Delta$, which is far from half filling. For $\mu = 0$ the LDOS $N^A(\varepsilon, \boldsymbol{i}_{\text{imp}})$ as a function of ε is shown in Fig. 4. One can see that if the chemical potential is close to half filling $\mu = 0$, the bound states do not appear. Therefore, one can conclude that whether or not an impurity in the S/AF bilayer becomes effectively magnetic depends on the value of the chemical potential. To understand the underlying physical reason let us consider the wave functions of Bloch electrons in a homogeneous superconductor in the presence of the staggered exchange field. They take the form

$$\begin{pmatrix}\hat{\psi}_{i\sigma}^A \\ \hat{\psi}_{i\sigma}^B\end{pmatrix}(\boldsymbol{p}) = \begin{pmatrix}\sqrt{1 + \sigma h/(\mu + \varepsilon)} \\ \sqrt{1 - \sigma h/(\mu + \varepsilon)}e^{-ip_y a_y}\end{pmatrix}e^{ip\boldsymbol{i}}, \quad (9)$$

where it is assumed that the unit cell is chosen along the y axis, and p_y and a_y are the electron momentum component and the lattice constant along this axis, respectively. We are mainly interested in the low energies $\varepsilon \sim \Delta$. If $\mu \gg \Delta$ the
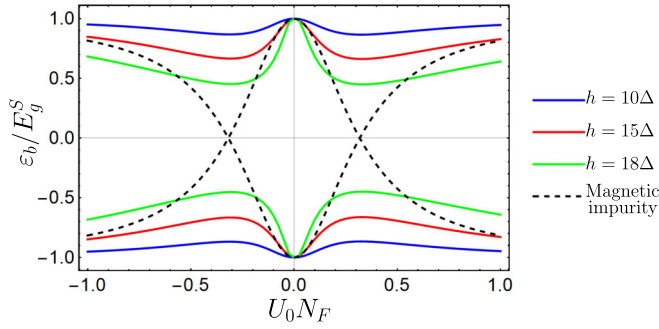
FIG. 3. Bound state energies as functions of the impurity strength. $\mu = 20\Delta$. Different colors correspond to different h. Dashed lines represent bound state energies at a magnetic impurity with the same strength in a conventional s-wave superconductor.

FIG. 5. Bound state energy ε_b in the plane (h, μ). The white region corresponds to fully suppressed superconductivity. $U_0 N_F = 0.3$.

probability density of spin-up electrons is presumably concentrated at sites A and the probability density of spin-down electrons is concentrated at sites B. Consequently, if the impurity is located at a site A, it interacts more strongly with spin-up electrons and vice versa [25]. This is the reason of the effectively magnetic behavior of nonmagnetic impurities in S/AF bilayers. In contrast, if $\mu = 0$, then at $\varepsilon < 0$ spin-up electrons are concentrated at A sites, but at $\varepsilon > 0$ spin-down electrons are concentrated there. Since all energies $\varepsilon \sim \Delta$ around the Fermi level contribute to superconducting pairing symmetrically, there is no difference in the spin-up and spin-down contribution to the interaction between the impurity and electrons. Therefore, impurities do not behave as effectively magnetic.

More quantitatively the regions of existence of the bound states and the dependence of the bound state energies on μ and h can be summarized in the form of the phase diagram presented in Fig. 5. In this figure the bound state energy ε_b is shown in the plane (h, μ). The white region corresponds to full suppression of superconductivity by the Néel exchange field of the AF layer. Although in the present paper the superconducting order parameter is not calculated self-consistently, the boundary of the superconductivity suppression in the

(h, μ) plane has already been calculated earlier [24]. From Fig. 5 it is seen that at small $\mu \lesssim \Delta$ the bound state indeed merges with the superconducting gap E_g^S for an arbitrary h. For larger μ the bound state appears. Its energy is governed by the parameter h/μ because it is this parameter which is responsible for making the impurity effectively magnetic [see Eq. (9)]. The impurity strength U_0 is chosen to provide maximal deviation of the bound state energy from the edge of the gap. In order to prove that the regions in the (h, μ) plane, where the bound states exist, do not depend qualitatively on the particular choice of U_0, and to provide more information on the phase diagram, we also plotted the curvature $|d^2\varepsilon_b/dU_0^2|_{U_0=0}|$ in the plane (h, μ) (see Appendix B). If this quantity is above zero, it indicates the existence of the bound states for a given set (h, μ) at an arbitrary value of U_0.

IV. SPATIAL STRUCTURE OF THE LDOS AROUND IMPURITY

Spatial structure of the LDOS around impurity at the energy of the bound state $\varepsilon = -\varepsilon_b$ is calculated according to Eq. (8) and is presented in Fig. 6. The spatial region occupied by the bound state has a spatial scale of the order of the superconducting coherence length $\xi \sim v_F/\Delta \sim 2at/\Delta$, where $v_F \sim 2at$ is the Fermi velocity of an electron in the normal state of the superconductor. The exponential decay is superimposed by a power-law suppression analogously to the case of magnetic impurities in conventional superconductors [1]. However, unlike the magnetic impurities in conventional superconductors here the LDOS has a "staggered" component, which oscillates between the sublattices. It is seen that if the impurity is localized at A site, the bound state LDOS is mainly concentrated at the B sublattice everywhere except for the atomic-scale region near the impurity site. This fact is closely connected with the spin polarization of the bound state LDOS. The spin-resolved impurity-induced LDOS is presented in Fig. 8 in Appendix C. It is seen that the bound states are indeed
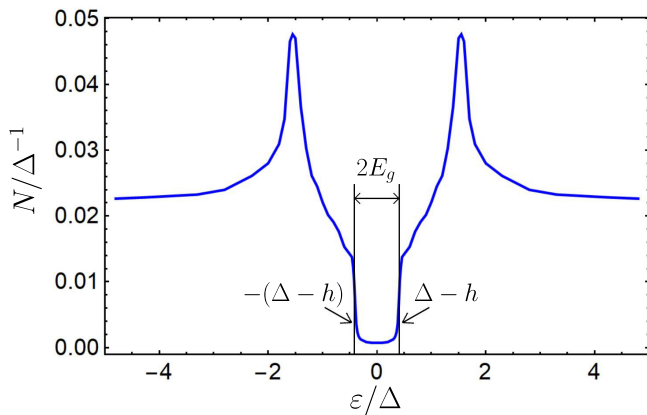

FIG. 4. LDOS as a function of energy. At $\mu = 0$ there is the only gap $2E_g = 2(\Delta - h)$. In this case both antiferromagnetic and superconducting gaps are open at the Fermi level and, therefore, $2E_g$ is of mixed origin. $\mu = 0$, $h = 0.6\Delta$, $U_0 = 10\Delta$.
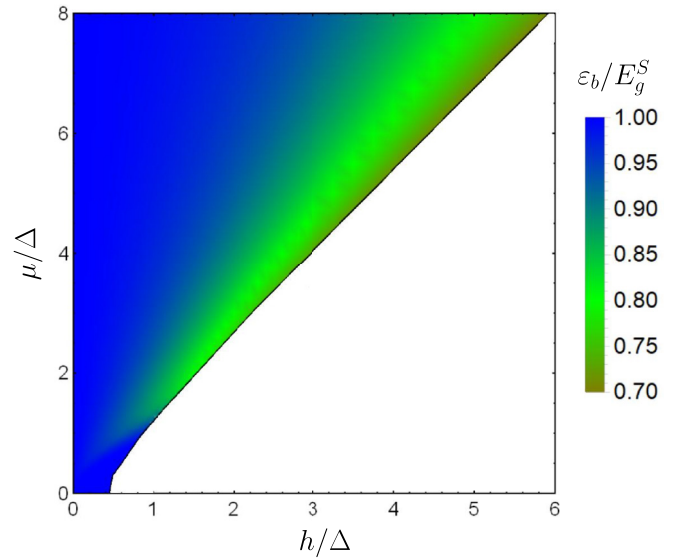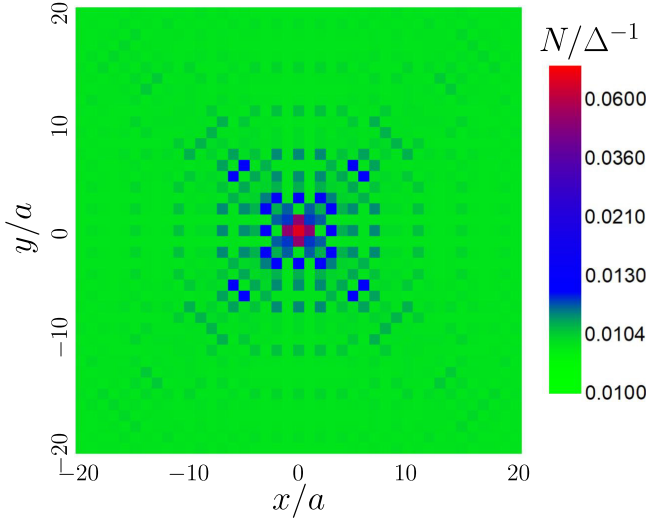
FIG. 6. LDOS at $\varepsilon = -\varepsilon_b$ as a function of coordinates. The impurity is at the A site of the unit cell $\boldsymbol{i}_{\mathrm{imp}} = (0,0)$. $\mu = 20\Delta$, $h = 15\Delta$, $U_0 = 10\Delta$.

spin split and if the impurity is at the A site the lower bound state $\varepsilon = -\varepsilon_b$ corresponds to the spin-down polarization (if the impurity is at the B site, the spin polarization of the bound states is reversed), as it is illustrated in Fig. 1. According to Eq. (1) it is energetically favorable to concentrate the DOS for spin-down electrons at the B sublattice to minimize the exchange energy.

Another interesting feature of the spatial structure of the bound state LDOS is that the overall decay of the LDOS and staggered oscillations associated with the sublattice structure are also superimposed by oscillations of a larger spatial scale compared to the atomic one, which is nevertheless significantly smaller than the superconducting coherence length scale. We associate these oscillations with the generation of finite-momentum Néel-type triplet correlations, which were
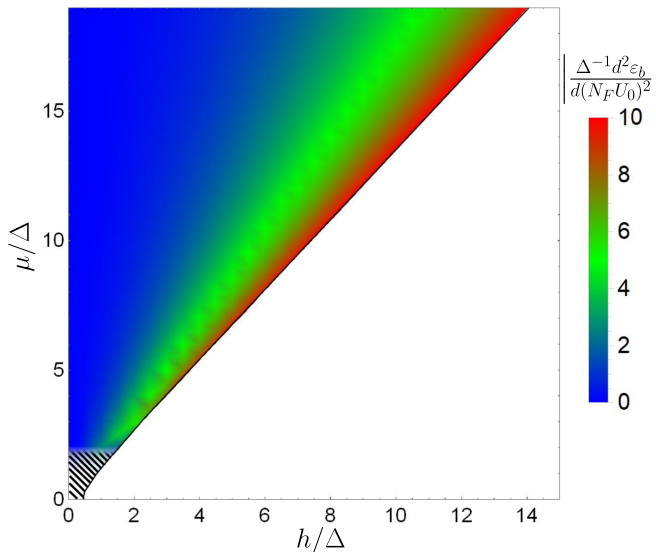

FIG. 7. $|d^2\varepsilon_b/dU_0^2|_{U_0=0}|$ in the plane (h, μ). The white region corresponds to fully suppressed superconductivity.
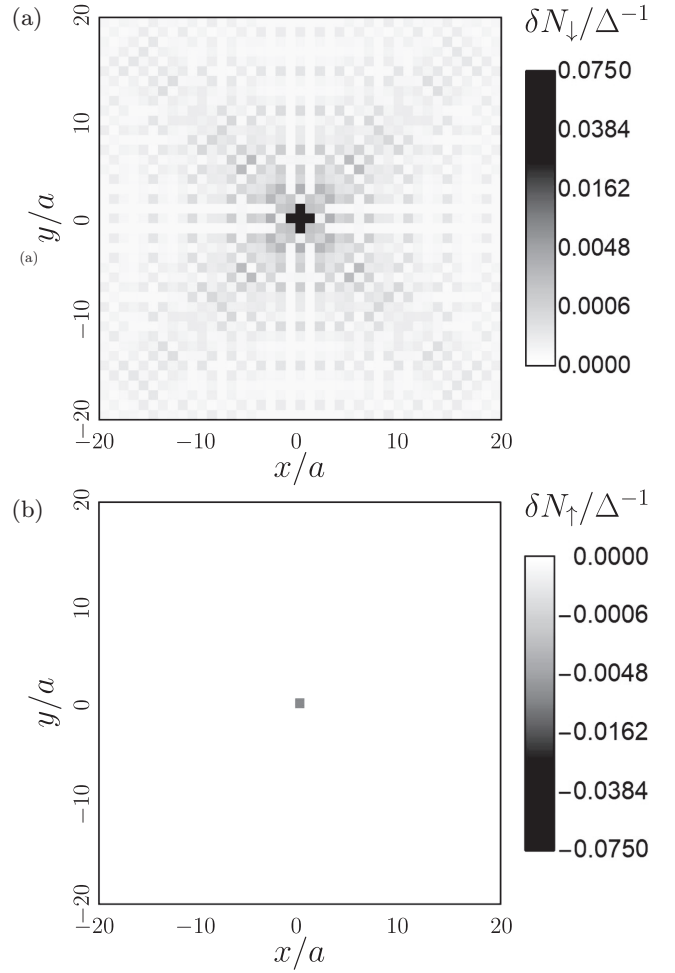

FIG. 8. Perturbation $\delta N_\sigma = N_\sigma - N_{0,\sigma}$ of the LDOS by the impurity. Here $N_{0,\sigma}$ is the LDOS at the same site in the absence of the impurity. (a) Spin-down local perturbation of the LDOS $\delta N_\downarrow$ and (b) spin-up perturbation $\delta N_\uparrow$. $\mu = 20\Delta$, $h = 15\Delta$, $U_0 = 10\Delta$.

originally predicted for S/AF bilayers with metallic antiferromagnets due to the Umklapp electron scattering processes at the AF/S interface [27]. The period of oscillations is $L_{\mathrm{osc}} = \pi v_F/\sqrt{\mu^2 - h^2}$. Data presented in Fig. 6 are calculated at $h = 1.5t$ and $\mu = 2t$. Then $L_{\mathrm{osc}} \approx 4a$, which is in agreement with the additional oscillation period seen in the figure. More detailed data proving that the reason for the appearance of the additional period of the LDOS oscillations is the finite-momentum Néel triplet pairing can be found in Appendix D. These data include the Fourier transform of Fig. 6, the explicit spatial structure of the Néel triplets demonstrating the same period. We also extracted the corresponding period for different (h, μ) points and checked that they are in excellent agreement with the analytical expression for L_{osc} (see Appendix D).

V. CONCLUSIONS

Based on the T-matrix approach we demonstrated that nonmagnetic impurities in S/AF heterostructures with conventional intraband s-wave pairing produce Andreev bound states. The physical reason is that the nonmagnetic impurities

in the presence of a staggered exchange field in the host material can behave as effectively magnetic due to the atomically oscillating, staggered, character of wave functions of conduction electrons. Whether or not an impurity in the S/AF bilayer becomes effectively magnetic depends on the value of the chemical potential. The bound states only exist at $\mu \gg T_{c0}$. It is in agreement with the behavior of the superconducting critical temperature of such systems in the presence of random disorder because it was shown earlier that only in this regime the nonmagnetic impurities are pair breaking for conventional s-wave superconductivity.

Analogously to the Yu-Shiba-Rusinov bound states the bound states in S/AF bilayers are spin split, but the spin of a particular bound state is determined by the sublattice to which the impurity belongs. The spatial structure of the bound state LDOS is also investigated. It is shown that the standard decay of the bound state LDOS is superimposed by atomic oscillations related to the staggered character of the exchange field in the host material and by another oscillating pattern produced by finite-momentum Néel triplet pairing generated at the impurity.

APPENDIX A: T-MATRIX APPROACH FOR TWO-SUBLATTICE GREEN'S FUNCTIONS

Calculations of the bound states and the LDOS have been performed in the framework of the T-matrix approach generalized for the antiferromagnetic host material. The general formalism of the Gor'kov Green's functions in the two-sublattice framework has been developed earlier [24,26]. The unit cell with two sites in it is chosen as shown in Fig. 1 of the main text. Introducing the two-sublattice Nambu spinor $\check{c}_i = (\hat{c}^A_{i,\uparrow}, \hat{c}^A_{i,\downarrow}, \hat{c}^B_{i,\uparrow}, \hat{c}^B_{i,\downarrow}, \hat{c}^{A\dagger}_{i,\uparrow}, \hat{c}^{A\dagger}_{i,\downarrow}, \hat{c}^{B\dagger}_{i,\uparrow}, \hat{c}^{B\dagger}_{i,\downarrow})^T$ and the Pauli matrices $\boldsymbol{\sigma} = (\sigma_x, \sigma_y, \sigma_z)^T$ in spin space, $\boldsymbol{\tau} = (\tau_x, \tau_y, \tau_z)^T$ in particle-hole space, and $\boldsymbol{\rho} = (\rho_x, \rho_y, \rho_z)^T$ in sublattice space, we define the retarded Green's function as

$$\check{G}_{ij}(t_1 - t_2) = -\begin{pmatrix} 1 & 0 \\ 0 & -i\sigma_y \end{pmatrix}_\tau \rho_x \Theta(t_1 - t_2)$$
$$\times \langle\{\check{c}_i(t_1), \check{c}_j^\dagger(t_2)\}\rangle \begin{pmatrix} 1 & 0 \\ 0 & -i\sigma_y \end{pmatrix}_\tau, \quad \text{(A1)}$$

where $\boldsymbol{i}$ is now the radius vector of the full unit cell, and subscript τ means that the explicit matrix structure corresponds to the particle-hole space. The Green's function is a 8×8 matrix in the direct product of spin, particle-hole, and sublattice spaces. We choose the z axis along $\boldsymbol{h}$. The Fourier-transformed Green's function $\check{G}_{ij}(\varepsilon) = \int e^{i\varepsilon(t_1-t_2)}\check{G}_{ij}(t_1-t_2)d(t_1-t_2)$ obeys the equation

$$(\check{H}_i^0 - \check{U}_i)\check{G}_{ij} = \delta_{ij}, \quad \text{(A2)}$$

where $\check{H}_i^0$ is the Hamiltonian of the homogeneous S/AF bilayer, which acts on the Green's function as follows:

$$\check{H}_i^0 \check{G}_{ij} = [(\varepsilon + i\Gamma)\tau_z + \mu + h\sigma_z\rho_z + \Delta i\tau_y]\rho_x\check{G}_{ij} + \check{K}_i\check{G}_{ij} \quad \text{(A3)}$$

where $\Gamma > 0$ is the Dynes parameter describing the broadening of the bound state peaks. $\check{K}_i$ is the kinetic term for nearest neighbor hopping

$$\check{K}_i\check{G}_{ij} = \rho_+ \sum_{\boldsymbol{a}} \check{G}_{\boldsymbol{i}+\boldsymbol{a}-\boldsymbol{a}_y,\boldsymbol{j}} + \rho_- \sum_{\boldsymbol{a}} \check{G}_{\boldsymbol{i}+\boldsymbol{a}+\boldsymbol{a}_y,\boldsymbol{j}} \quad \text{(A4)}$$

and $\boldsymbol{a} \in \{\pm\boldsymbol{a}_x, \pm\boldsymbol{a}_y, \pm\boldsymbol{a}_z\}$. $\check{U}_i$ is the potential of the impurity, which in the two-sublattice formalism takes the form

$$\check{U}_i = \check{U}_0\delta_{\boldsymbol{i},\boldsymbol{i}_{\text{imp}}} = U_0\frac{(\rho_x + \nu i\rho_y)}{2}\delta_{\boldsymbol{i},\boldsymbol{i}_{\text{imp}}}, \quad \text{(A5)}$$

where $\nu = \pm 1$ if the impurity is located at the A (B) site.

The standard T-matrix ansatz for the full Green's function takes the form

$$\check{G}_{ij} = \check{G}_{ij}^0 + \sum_{m,l} \check{G}_{im}^0 \check{T}_{ml} \check{G}_{lj}^0, \quad \text{(A6)}$$

where $\check{G}_{i,j}^0$ is the Green's function of the homogeneous S/AF bilayer in the absence of impurity obeying

$$\check{H}_i^0 \check{G}_{ij}^0 = \delta_{ij}. \quad \text{(A7)}$$

Subtracting perturbed (A2) and unperturbed (A7) equations, and multiplying by H_j^0 from the right, we obtain

$$\check{T}_{ij} - \check{U}_i \sum_m \check{G}_{il}^0 \check{T}_{lj} - \check{U}_i\delta_{ij} = 0. \quad \text{(A8)}$$

Due to isotropy of the impurity potential we can write

$$\check{T}_{ij} = \check{T}^0\delta_{\boldsymbol{i},\boldsymbol{i}_{\text{imp}}}\delta_{\boldsymbol{j},\boldsymbol{i}_{\text{imp}}}. \quad \text{(A9)}$$

Then from Eq. (A8) it follows that

$$\check{T}^0 = \left(1 - \check{U}_0\check{G}_{\boldsymbol{i}_{\text{imp}},\boldsymbol{i}_{\text{imp}}}^0\right)^{-1}\check{U}_0. \quad \text{(A10)}$$

Energy of the bound states is determined by the poles of the T matrix, that is, the bound state energies are obtained from the following equation:

$$\det\left(1 - \check{U}_0\check{G}_{\boldsymbol{i}_{\text{imp}},\boldsymbol{i}_{\text{imp}}}^0\right) = 0. \quad \text{(A11)}$$

The spin-resolved LDOS at A and B sites of the $\boldsymbol{i}$th unit cell is determined via the imaginary part of the retarded Green's function

$$N_{\uparrow,\downarrow}^{A,B}(\varepsilon, \boldsymbol{i})$$
$$= -\frac{1}{\pi}\text{Im}\left\{\text{Tr}\left[\frac{\check{G}_{ii}(\sigma_0 + s\sigma_z)(\tau_0 + \tau_z)(\rho_x + \nu i\rho_y)}{8}\right]\right\}, \quad \text{(A12)}$$

where $s = \pm 1$ for spin $\uparrow$ ($\downarrow$) and $\nu = \pm 1$ for A (B) sublattices. The Green's function $\check{G}_{ii}$ is calculated according to Eqs. (A6), (A9), and (A10). The homogeneous Green's function $\check{G}_{ij}^0$ can be calculated analytically,

$$\check{G}_{ij}^0 = \int \frac{d^3\boldsymbol{p}}{(2\pi)^3} e^{\frac{ip_ya_y\rho_z}{2}} \check{G}^0(\boldsymbol{p}) e^{\frac{-ip_ya_y\rho_z}{2}} e^{i\boldsymbol{p}(i-j)}, \quad \text{(A13)}$$

and $\check{G}^0(\boldsymbol{p})$ should be found from the unperturbed Gor'kov equation in the momentum representation:

$$(\varepsilon\tau_z + \mu + h\sigma_z\rho_z + i\tau_y\Delta)\rho_x\check{G}^0(\boldsymbol{p})$$
$$- 2t[\cos(p_xa) + \cos(p_ya)]\check{G}^0(\boldsymbol{p}) = 1. \quad (A14)$$

Then $\check{G}_{ij}^0$ is diagonal in spin space, that is, $\check{G}_{ij}^0 = \check{G}_{ij,\uparrow}^0(1 + \sigma_z)/2 + \check{G}_{ij,\downarrow}^0(1 - \sigma_z)/2$, and each of the components in spin space can be expanded over Pauli matrices in particle-hole and sublattice spaces:

$$G_{ij,\sigma}^0 = G_{0x}^\sigma\tau_0\rho_x + G_{yx}^\sigma\tau_y\rho_x + G_{zx}^\sigma\tau_z\rho_x + G_{0y}^\sigma\tau_0\rho_y$$
$$+ G_{yy}^\sigma\tau_y\rho_y + G_{zy}^\sigma\tau_z\rho_y \quad (A15)$$

with

$$G_{0x}^\sigma = \mu[(-h^2 + \Delta^2 - \varepsilon^2 + \mu^2)I_1 - I_2]$$
$$G_{yx}^\sigma = -i\Delta[(-h^2 + \Delta^2 - \varepsilon^2 + \mu^2)I_1 + I_2]$$
$$G_{zx}^\sigma = \varepsilon[(-h^2 - \Delta^2 + \varepsilon^2 - \mu^2)I_1 - I_2]$$
$$G_{0y}^\sigma = 2i\sigma h\varepsilon\mu I_1$$
$$G_{yy}^\sigma = 2\sigma h\Delta\varepsilon I_1$$
$$G_{zy}^\sigma = i\sigma h[(h^2 - \Delta^2 - \varepsilon^2 - \mu^2)I_1 + I_2] \quad (A16)$$

where $I_1 = -\frac{2\sqrt{2}i\pi}{(\alpha_1+\alpha_2)\alpha_1\alpha_2}$, $I_2 = \frac{\sqrt{2}i\pi}{\alpha_1+\alpha_2}$, $\alpha_{1,2} = \sqrt{-\beta_1 \mp \sqrt{\beta_1^2 - 4\beta_0}}$, $\beta_0 = h^4 + (\Delta^2 - \varepsilon^2 + \mu^2)^2 - 2h^2(\Delta^2 + \varepsilon^2 + \mu^2)$, and $\beta_1 = 2(\Delta^2 - \varepsilon^2 - \mu^2 + h^2)$.

APPENDIX B: PHASE DIAGRAM

In order to provide more information on the phase diagram of the bound state existence in Fig. 7 we present the curvature $|d^2\varepsilon_b/dU_0^2|_{U_0=0}|$ in the plane (h, μ). If this quantity is more than zero, it indicates the existence of the bound states for a given set (h, μ) at an arbitrary value of U_0. This figure shows the same trends as Fig. 5, thus indicating that the regions of existence/absence of the bound states do not depend qualitatively on the particular value of U_0. The shaded area corresponds to the region of small μ, where the bound states do not exist at all values of U_0 and, therefore, it is not possible to determine the curvature.

APPENDIX C: SPIN STRUCTURE OF THE BOUND STATE LDOS

In order to prove that the Andreev bound states generated by a nonmagnetic impurity are spin resolved, in Fig. 8 we plot the spin-resolved LDOS at $\varepsilon = -\varepsilon_b$. Only the perturbation δN_σ of the LDOS by the impurity is shown. Here $\delta N_\sigma = N_\sigma - N_{0,\sigma}$, where $N_{0,\sigma}$ is the LDOS at the same site in the absence of the impurity. It manifests a perfect staggered order. In Fig. 8 the nonmagnetic impurity is located at the A site. It is seen that in this case only the spin-down LDOS $N_\downarrow$ is perturbed by the impurity for the lower bound state $-\varepsilon_b$, except for the impurity site. Directly at the impurity site we see very local perturbation of the LDOS in the spin-up subband, which results from the fact that the nonmagnetic impurity by itself works as an on-site perturbation of the chemical potential.
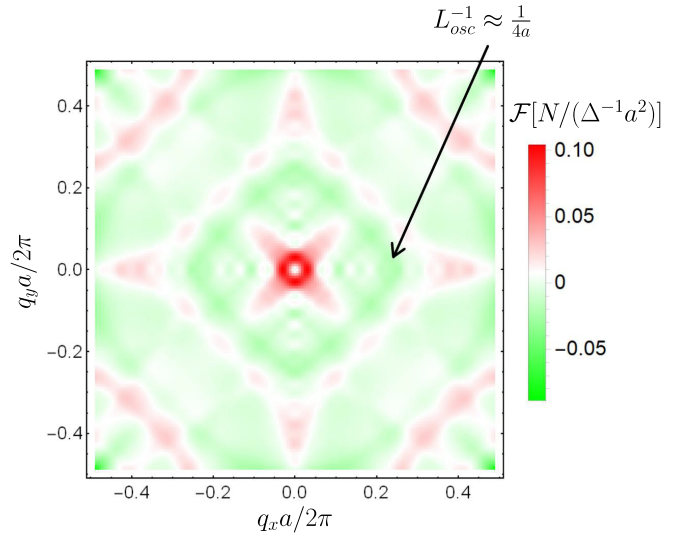

FIG. 9. Fourier transform of the LDOS presented in Fig. 6. $\varepsilon = -\varepsilon_b$. The impurity is at the A site. $\mu = 20\Delta$, $h = 15\Delta$, $U_0 = 10\Delta$.

APPENDIX D: SPATIAL OSCILLATIONS OF THE LDOS

Here we provide more detailed data that prove that the reason for the appearance of the additional period of the LDOS oscillations is the finite-momentum Néel triplet pairing. In Fig. 9 we demonstrate the Fourier transform of the LDOS data presented in Fig. 6. The peak corresponding to the oscillation period $L_{osc} \approx 4a$ is clearly seen as a green ring curve. Also in Fig. 6 we see two additional specific features. The largest green ring curve approximately having radius $qa \approx \pi$ represents the Néel staggered order of the LDOS. The central red ring curve of the smallest radius originates from the overall decay of the impurity-induced LDOS at the length scale ξ. The fourfold-symmetric anisotropy of the image is due to the fact that we consider the square lattice.

In Fig. 10 we additionally demonstrate the oscillation period L_{osc} extracted from the LDOS for different points in the (h, μ) space. The dashed line represents the formula $L_{osc} = \pi v_F/\sqrt{\mu^2 - h^2}$. It is seen that the data are in excellent
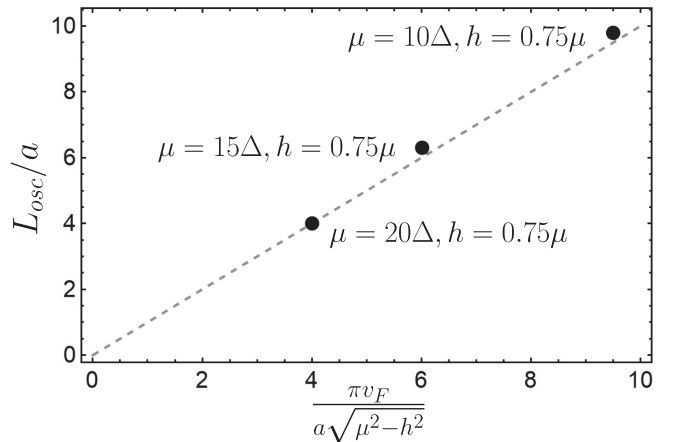

FIG. 10. L_{osc} extracted from the LDOS for different points in the (h, μ) space, denoted by the black circles. The dashed line represents the formula $L_{osc} = \pi v_F/\sqrt{\mu^2 - h^2}$.
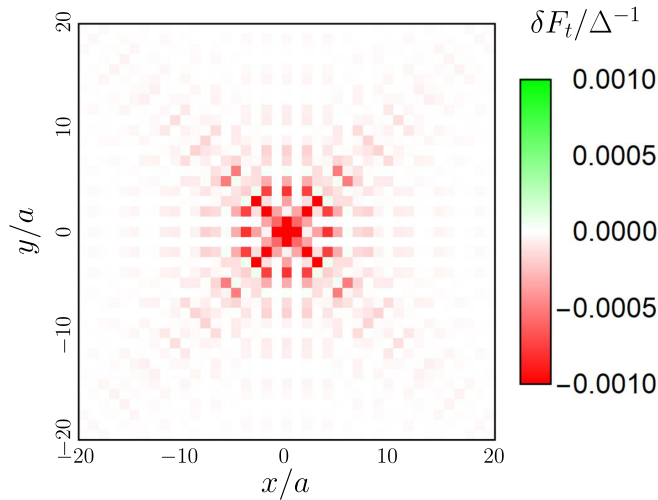
FIG. 11. Impurity-induced perturbation δF_t of the ideal Néel triplet correlation structure at $\varepsilon = -\varepsilon_b$. The impurity is at the A site. $\mu = 20\Delta, h = 15\Delta, U_0 = 10\Delta$.

agreement with this dependence. Moreover, as it was already indicated in Sec. IV, the period increases as μ decreases. This suggests that this periodic pattern cannot be ascribed to the Friedel oscillations because in the framework of the considered tight-binding model on a square lattice the period of Friedel oscillations does not manifest such a monotonic dependence on μ.

Also in Fig. 11 we demonstrate the perturbation in the spatial structure of the Néel-type triplet correlations induced by the impurity. The perturbation is defined as $\delta F_t(\varepsilon) = F_t(\varepsilon) - F_t^0(\varepsilon)$, where $F_t^{A,B}(\varepsilon) = (1/8)\mathrm{Tr}[\check{G}_{ii}(\varepsilon)(\tau_x - i\tau_y)\sigma_z(\rho_x + i\nu\rho_y)]$ is the anomalous component of the retarded Green's function and $F_t^{0A,B}(\varepsilon) = (1/8)\mathrm{Tr}[\check{G}_{ii}^0(\varepsilon)(\tau_x - i\tau_y)\sigma_z(\rho_x + i\nu\rho_y)]$ is the anomalous component of the homogeneous Green's function in the absence of the impurity. The Green's function δF_t in Fig. 11 is a sum of the both sublattices. The anomalous Green's function is plotted at $\varepsilon = -\varepsilon_b$. The rings corresponding to the oscillations of the amplitude of the Néel triplet pairs with the period $L_{\mathrm{osc}} \approx 4a$ are seen in this figure.

[1] A. V. Balatsky, I. Vekhter, and J.-X. Zhu, Impurity-induced states in conventional and unconventional superconductors, Rev. Mod. Phys. **78**, 373 (2006).

[2] A. Yazdani, B. A. Jones, C. P. Lutz, M. F. Crommie, and D. M. Eigler, Probing the local effects of magnetic impurities on superconductivity, Science **275**, 1767 (1997).

[3] E. W. Hudson, K. M. Lang, V. Madhavan, S. H. Pan, H. Eisaki, S. Uchida, and J. C. Davis, Interplay of magnetism and high-T_c superconductivity at individual Ni impurity atoms in $Bi_2Sr_2CaCu_2O_{8+\delta}$, Nature (London) **411**, 920 (2001).

[4] S. Grothe, S. Chi, P. Dosanjh, R. Liang, W. N. Hardy, S. A. Burke, D. A. Bonn, and Y. Pennec, Bound states of defects in superconducting life as studied by scanning tunneling spectroscopy, Phys. Rev. B **86**, 174503 (2012).

[5] S. Nadj-Perge, I. K. Drozdov, J. Li, H. Chen, S. Jeon, J. Seo, A. H. MacDonald, B. A. Bernevig, and A. Yazdani, Observation of Majorana fermions in ferromagnetic atomic chains on a superconductor, Science **346**, 602 (2014).

[6] R. Pawlak, M. Kisiel, J. Klinovaja, T. Meier, S. Kawai, T. Glatzel, D. Loss, and E. Meyer, Probing atomic structure and Majorana wavefunctions in mono-atomic Fe chains on superconducting Pb surface, npj Quantum Inf. **2**, 16035 (2016).

[7] L. Schneider, P. Beck, T. Posske, D. Crawford, E. Mascot, S. Rachel, R. Wiesendanger, and J. Wiebe, Topological Shiba bands in artificial spin chains on superconductors, Nat. Phys. **17**, 943 (2021).

[8] P. W. Anderson, Theory of dirty superconductors, J. Phys. Chem. Solids **11**, 26 (1959).

[9] A. Abrikosov and L. Gor'kov, Contribution to the theory of superconducting alloys with paramagnetic impurities, Sov. Phys. JETP **12**, 1243 (1961).

[10] V. P. Mineev and K. V. Samokhin, *Introduction to Unconventional Superconductivity* (Gordon and Breach, New York, 1999).

[11] K. Michaeli and L. Fu, Spin-orbit locking as a protection mechanism of the odd-parity superconducting state against disorder, Phys. Rev. Lett. **109**, 187003 (2012).

[12] D. C. Cavanagh and P. M. R. Brydon, Robustness of unconventional s-wave superconducting states against disorder, Phys. Rev. B **101**, 054509 (2020).

[13] D. C. Cavanagh and P. M. R. Brydon, General theory of robustness against disorder in multiband superconductors, Phys. Rev. B **104**, 014503 (2021).

[14] D. Dentelski, V. Kozii, and J. Ruhman, Effect of interorbital scattering on superconductivity in doped Dirac semimetals, Phys. Rev. Res. **2**, 033302 (2020).

[15] T. Sato and Y. Asano, Superconductivity in Cu-doped Bi_2Se_3 with potential disorder, Phys. Rev. B **102**, 024516 (2020).

[16] Y. Luh, Bound state in superconductors with paramagnetic impurities, Acta Phys. Sin. **21**, 75 (1965).

[17] H. Shiba, Classical spins in superconductors, Prog. Theor. Phys. **40**, 435 (1968).

[18] A. I. Rusinov, On the theory of gapless superconductivity in alloys containing paramagnetic impurities, Sov. Phys. JETP **29**, 1101 (1969).

[19] A. V. Balatsky, M. I. Salkola, and A. Rosengren, Impurity-induced virtual bound states in d-wave superconductors, Phys. Rev. B **51**, 15547 (1995).

[20] W.-F. Tsai, Y.-Y. Zhang, C. Fang, and J. Hu, Impurity-induced bound states in iron-based superconductors with s-wave $\cos k_x \cdot \cos k_y$ pairing symmetry, Phys. Rev. B **80**, 064513 (2009).

[21] D.-D. Wang, B. Liu, M. Liu, Y.-F. Yang, and S.-P. Feng, Impurity-induced bound states as a signature of pairing symmetry in multiband superconducting $CeCu_2Si_2$, Front. Phys. **14**, 13501 (2019).

[22] Y. Zhu, N. A. Hackner, and P. M. R. Brydon, Bound states around impurities in a superconducting bilayer, Phys. Rev. B **107**, 134514 (2023).

[23] A. I. Buzdin and L. N. Bulaevskǐ, Antiferromagnetic superconductors, Sov. Phys. Usp. **29**, 412 (1986).

[24] G. A. Bobkov, I. V. Bobkova, and A. M. Bobkov, Proximity effect in superconductor/antiferromagnet hybrids: Néel triplets and impurity suppression of superconductivity, Phys. Rev. B **108**, 054510 (2023).

[25] E. H. Fyhn, A. Brataas, A. Qaiumzadeh, and J. Linder, Superconducting proximity effect and long-ranged triplets in dirty metallic antiferromagnets, Phys. Rev. Lett. **131**, 076001 (2023).

[26] G. A. Bobkov, I. V. Bobkova, A. M. Bobkov, and A. Kamra, Néel proximity effect at antiferromagnet/superconductor interfaces, Phys. Rev. B **106**, 144512 (2022).

[27] G. A. Bobkov, V. M. Gordeeva, A. M. Bobkov, and I. V. Bobkova, Oscillatory superconducting transition temperature in superconductor/antiferromagnet heterostructures, Phys. Rev. B **108**, 184509 (2023).